International Conference on Mathematics and Computational Methods Applied to Nuclear Science & Engineering (M&C 2013), Sun Valley, Idaho, USA, May 5-9, 2013, on CD-ROM, American Nuclear Society, LaGrange Park, IL (2013)

A GENERALIZED FRAMEWORK FOR IN-LINE ENERGY DEPOSITION DURING STEADY-STATE MONTE CARLO RADIATION TRANSPORT

David P. Griesheimer
Bettis Atomic Power Laboratory
P.O. Box 79, West Mifflin, PA 15122
david.griesheimer.contractor@unnpp.gov

Mark H. Stedry
Knolls Atomic Power Laboratory
P.O. Box 1072, Schenectady, NY 12301
mark.stedry.contractor@unnpp.gov

ABSTRACT

A rigorous treatment of energy deposition in a Monte Carlo transport calculation, including coupled transport of all secondary and tertiary radiations, increases the computational cost of a simulation dramatically, making fully-coupled heating impractical for many large calculations, such as 3-D analysis of nuclear reactor cores. However, in some cases, the added benefit from a full-fidelity energy-deposition treatment is negligible, especially considering the increased simulation run time. In this paper we present a generalized framework for the in-line calculation of energy deposition during steady-state Monte Carlo transport simulations. This framework gives users the ability to select among several energy-deposition approximations with varying levels of fidelity. The paper describes the computational framework, along with derivations of four energy-deposition treatments. Each treatment uses a unique set of self-consistent approximations, which ensure that energy balance is preserved over the entire problem. By providing several energy-deposition treatments, each with different approximations for neglecting the energy transport of certain secondary radiations, the proposed framework provides users the flexibility to choose between accuracy and computational efficiency. Numerical results are presented, comparing heating results among the four energy-deposition treatments for a simple reactor/compound shielding problem. The results illustrate the limitations and computational expense of each of the four energy-deposition treatments.

Key Words: Monte Carlo, Reactor, Heating, Energy Deposition, Feedback, In-Line

1. INTRODUCTION

Energy deposition in neutron and photon transport problems is a complicated process. Each of the possible radiation interaction mechanisms has a unique Q-value, which gives the energy gain or loss that will occur during the reaction. In addition, many reactions, such as fission, produce secondary particles, which cause energy to be transported away from the site of the reaction rather than being deposited locally. Furthermore, many nuclear reactions involve a change in the form of the energy during the reaction. For example, radiative neutron capture reactions result in the loss of neutron kinetic energy but the production of one or more secondary photons, which transport energy away from the capture site. As such, rigorous energy deposition calculations require the solution of a coupled set of neutron and photon transport problems, which can be computationally expensive. In Monte Carlo (MC) methods, the process of energy transfer is further compounded by the use of non-analog variance reduction schemes. For example, implicit

capture MC transport algorithms do not attempt to preserve energy for each reaction, or even for each particle history. Instead, as an unbiased technique, the algorithms are designed to preserve energy, on average, over all reactions and particle histories.

The use of MC methods for radiation heating calculations is not new. In fact, many contemporary MC transport codes, including MCNP [1], support in-line coupled transport calculations including neutrons, photons, and/or electrons. However, experience with these codes over the years has shown that a rigorous treatment of energy deposition in a MC transport calculation, including coupled transport of all secondary radiations, increases the computational cost of a simulation dramatically. As a result, fully-coupled heating is often impractical for large calculations, such as 3D analysis of nuclear reactors. Also, in many cases, the added benefit from a full-fidelity energy treatment is not worth the increased calculation time. For example, in light-water fission reactors, upwards of 88% of the total energy is deposited directly at the fission site, with an additional 3% transported away as neutrons and 9% as photons. For many reactor calculations, simply assuming that all of the energy is deposited locally at the fission site will produce a reasonable (and conservative) estimate of the local heating within the core. However, such an assumption will not account for the direct heating of coolant and structural materials in the core, which may be important in other types of reactor analysis calculations.

As a result of the need for different levels of accuracy in the energy deposition treatment, we have developed a generalized framework for the in-line treatment of energy deposition in MC transport calculations. This framework gives users the ability to select among several energy-deposition treatments with varying levels of fidelity. This paper describes the general computational framework, along with derivations of four energy-deposition treatments. Each treatment uses a unique set of self-consistent approximations, which ensure that energy balance is satisfied over the entire problem. By providing several energy deposition treatments, each with different approximations for neglecting the energy transport of certain secondary radiations, the proposed framework provides users the flexibility to choose between accuracy and computational efficiency. Numerical results presented in Section 6 illustrate the limitations and computational expense of each of the four energy-deposition treatments. Based on these results we conclude that the new common framework provides much needed flexibility to end-users of MC radiation transport. Allowing users to tailor the accuracy of the energy deposition treatment to a particular application or to meet resource limitations has the potential to increase computational throughput and/or enable analysis of larger models than were previously possible.

2. ENERGY RELEASE, TRANSFER, AND DEPOSITION

Radiative heating calculations are complex because the radiation energy can be transferred many times and converted into several different forms before it is ultimately deposited and converted to heat within a material. Therefore, we begin by outlining the different methods by which energy is created, transferred, and ultimately deposited by radiation.

2.1. Energy Release Mechanisms

Within a fission reactor the primary energy release mechanism is neutron-induced fission, which is a highly-exothermic reaction, with every fission event releasing approximately 200 MeV of sensible energy [2]. A portion (~90%) of this energy is released immediately as photons and

kinetic energy of fission fragments and free neutrons. The remaining fission energy is stored as potential energy in the nucleus of the radioactive fission products. This energy is released some time after the fission event as the fission products undergo radioactive decay and emit charged particles, photons, and/or delayed neutrons, which carry away the excess energy. For ^{235}U, less than 10% of the sensible energy produced in fission is stored in fission products and will appear later as delayed radiation. Because neutrinos do not readily interact with matter, the energy released as neutrinos is typically neglected. In this paper, the sensible energy release in fission will be denoted $\bar{Q}_{\mathrm{f}}(E)$, where the overbar indicates that the energy release is a weighted average over all fissionable nuclides. We will also denote the fraction of energy carried away by each type of particle by the variable f_i, where *i* is the particle/radiation type exiting the fission event. Presently, the ENDF format [4] provides energy release data for fission fragments (f_{fpke}), prompt neutrons ($f_{\mathrm{prompt\ n}}$), prompt photons ($f_{\mathrm{prompt}\ \gamma}$), beta particles ($f_{\mathrm{beta}}$), delayed neutrons ($f_{\mathrm{delayed\ n}}$), and delayed photons ($f_{\mathrm{delayed}\ \gamma}$). In this paper, we assume that the absolute energy release values from ENDF have been normalized by $\bar{Q}_{\mathrm{f}}(E)$ so that the fractional release values sum to 1.0.

In addition to the energy produced by fission, which is the dominant source in nuclear reactors, there are many exothermic neutron/nucleus reactions that can occur as free neutrons interact within the reactor. Such interactions typically involve the formation and subsequent radioactive decay (either instantaneous or delayed) of a compound nucleus during a neutron capture event. In the nuclear reactor community, the energy released during these exothermic reactions is often referred to as indirect energy production, and typically accounts for 1% to 6% of the total energy output of a reactor [2]. In this paper, the energy released during (non-fission) neutron/nucleus interactions will be denoted $\bar{Q}_{\mathrm{nf}}(E)$, where the overbar indicates that the energy release is a weighted average over all non-fission reactions. A positive value for $\bar{Q}_{\mathrm{nf}}(E)$ indicates a net energy release due to the neutron/nucleus interaction while a negative value indicates a net energy loss. Negative values for $\bar{Q}_{\mathrm{nf}}(E)$ occur when the binding energy of the product(s) of a neutron/nucleus interaction is larger than the binding energies of the individual reactants. It is important to note that, in this analysis, $\bar{Q}_{\mathrm{nf}}(E)$ applies to neutron interactions only. While some photon interactions, such as photodisintegration, can lead to a net gain or loss of available energy, the effects of these reactions are small for reactor heating applications, and will be neglected in this paper.

2.2. Energy Deposition

During radiation transport energy is converted from one form to another until it is ultimately transferred into kinetic energy of molecules in the surrounding material, converting the energy into heat. In this paper, we will refer to this final conversion of energy into heat as energy deposition. In nuclear reactors, energy deposition is primarily due to the slowing down of fission fragments, beta particles, electrons (produced from photon interactions), and recoil nuclei.

In many applications, it is convenient to distinguish between energy deposition due to fission, neutron slowing-down (including non-fission capture reactions), and photon interactions. Fission energy deposition includes kinetic energy transfer due to fission fragment and decay beta particle slowing-down following a fission event. Neutron slowing-down interactions include both direct kinetic energy transfer due to neutron/nucleus collisions as well as local kinetic energy deposition of charged particles emitted after a neutron capture event. Strictly speaking,

neutron slowing-down deposition does not include the energy of photons created in capture or inelastic scattering events, since these photons will typically carry their energy away from the interaction site. Energy deposition due to photon interactions is caused by kinetic energy transfer due to slowing down of charged particles (electrons and/or positrons) produced in photon/atom interactions.

Each reaction type deposits some amount of energy, depending on the type and kinematics of the reaction. Therefore, it follows that the total energy deposited by each form of radiation is proportional to the reaction rates for each of the interaction mechanisms. As a result, it is convenient to express energy deposition data as a microscopic cross section, expressed in eV·barns, which is referred to as the KERMA (Kinetic Energy Release in Materials) [3]. KERMA values are calculated using either a direct or energy-balance method [3] and are available for most nuclides and reaction types [3, 4]. In this paper we will denote KERMA values for radiation of type x (neutron or photon of energy E) undergoing reaction j with nuclide i, by $h_{x,i,j}(E)$. However, in the derivations that follow it is often more convenient to work with average KERMA values computed over each of the three energy deposition categories: fission, non-fission (neutron slowing-down), and photon.

In this paper we will define $\bar{h}_{\mathrm{f}}$ as the average fission KERMA over all fissionable nuclides. The average fission KERMA value can be computed by averaging the KERMA values for the individual nuclides, or based on the average energy released per fission ($\bar{Q}_{\mathrm{f}}$) and the fraction of that energy carried off by fission fragments (f_{fpke}) and beta particles (f_{beta}),

$$\bar{h}_{\mathrm{f}}(E) = \sum_i \rho_i h_{\mathrm{n},i,\mathrm{f}}(E) = \sum_i \left(f_{\mathrm{fpke},i} + f_{\mathrm{beta},i} \right) \Sigma_{\mathrm{f},i} \bar{Q}_{\mathrm{f},i}(E), \tag{1}$$

where ρ_i is the number density of nuclide i. Similarly, we can define $\bar{h}_{\mathrm{nf}}$ and $\bar{h}_{\gamma}$ as the average non-fission and photon KERMAs, respectively. In each case, the average KERMA is equal to the density weighted sum of KERMA values taken over all nuclides i and all non-fission reactions j

$$\bar{h}_{\mathrm{nf}}(E) = \sum_i \sum_j \rho_i h_{\mathrm{n},i,j}(E), \tag{2}$$

$$\bar{h}_{\gamma}(E) = \sum_i \sum_j \rho_i h_{\gamma,i,j}(E), \tag{3}$$

where ρ_i is the number density of nuclide i. Based on the definitions given in Eqs. (1)-(3), the total energy deposited by each reaction category is equal to the corresponding radiation flux times the average KERMA value and integrated over all energies.

3. ENERGY DEPOSITION EQUATIONS

During radiation transport energy may change forms several times before ultimately being deposited in, or escaping from, the problem. Thus, a complete description of the radiative energy transfer and deposition process requires a coupled set of neutron, photon, and charged particle transport equations. In addition, the build-up and decay of radioactive nuclides, which act as temporary storage for potential energy in the system, create complex time dependencies within

the problem. As a result, solving the complete energy deposition problem can be computationally expensive, which limits the use of in-line heating calculations for routine reactor design or analysis.

For reactor heating applications, we can simplify the energy deposition equations with several basic assumptions. First, we assume that charged particles deposit their energy where they are created. This assumption eliminates the charged particle transport process and removes one of the three coupled equations. For nuclear reactors the energy redistribution due to charged particle transport is negligible and this assumption does not cause any meaningful loss of accuracy. However, when eliminating explicit charged particle transport, the remaining neutron and photon transport equations and KERMA values must be modified to account for neglected effects (such as bremsstrahlung and the production of annihilation photons due to electron/positron pairs). For this analysis, we will also neglect photoneutron production terms in order to eliminate two-way coupling between the neutron and photon transport equations. This simplification allows the heating equations to be solved with only one neutron and one photon transport calculation. Including photodisintegration reactions creates a dependency between the neutron source term and the photon flux, which, in turn, requires iteration between the neutron and photon transport equations.

We will also assume that the reactor is operating at steady-state condition and that the concentrations of all radioactive fission products have reached their equilibrium values. This assumption eliminates the time dependence of the energy deposition equations and allows radioactive decay to be treated as an instantaneous process. While this assumption is reasonable for reactors that have operated continuously at a constant power level for an extended period of time, it is not valid in the initial months after a startup or for reactors with a rapidly varying power history. In these cases, the assumption of instantaneous decay will tend to overpredict heating by several percent. However, because this overprediction is conservative from a reactor protection standpoint, this assumption is reasonable for many types of reactor analyses.

Finally, we will assume that the production yield and spectrum of secondary radiations (neutrons and photons) are separable. This assumption is commonly used in radiation transport, especially for the fission process, where the number of neutrons released per fission, $\bar{\nu}$, and the fission spectrum $\chi(E)$ are nearly always assumed to be independent. In MC transport, this assumed separability means that there is no guarantee that the total energy of neutrons or photons produced during a reaction will be equal to the average radiation energy released for that reaction. This issue complicates energy balance in MC calculations, making analog energy transport impractical for large MC calculations. In order to preserve energy balance over all particle histories (and generations for eigenvalue calculations), we utilize energy rebalance factors, discussed in Section 4, which ensure that the radiative energy emitted during a reaction is equal to the energy carried away by the secondary particle.

Based on these assumptions, we can write down a coupled set of integro-differential equations for the neutron and photon flux, which are given by

$$\int_{4\pi} \hat{\Omega}\cdot\nabla\psi_{\mathrm{n}}\left(E,\hat{\Omega}\right)d\hat{\Omega}+\Sigma_{\mathrm{t}}\phi_{\mathrm{n}}\left(E\right)=\int_{0}^{\infty}\Sigma_{\mathrm{s},E'\to E}\phi_{\mathrm{n}}\left(E'\right)dE'+S_{\mathrm{n}}\left(E\right),\ \text{and} \tag{4}$$

$$\int_{4\pi} \hat{\Omega}\cdot\nabla\psi_\gamma\left(E,\hat{\Omega}\right)d\hat{\Omega}+\mu_{\mathrm{t}}\phi_\gamma\left(E\right)=\int_0^\infty \mu_{\mathrm{s},E'\to E}\phi_\gamma\left(E'\right)dE'+S_\gamma\left(E\right), \tag{5}$$

respectively, where ψ is the angular flux, ϕ is the scalar flux, and all other symbols have their usual meanings. For brevity, the spatial dependence of the equations is not shown explicitly, but is assumed. In addition, the energy dependence of the macroscopic neutron (Σ) and photon (μ) cross sections is not shown explicitly but also is implied. Equations (4) and (5) are coupled by their source terms, which are given by (neglecting photoneutron production)

$$S_{\mathrm{n}}\left(E\right)=\frac{1}{k_{\mathrm{eff}}}\chi_{\mathrm{n,f}}\left(E\right)\int_0^\infty \bar{\nu}\left(E'\right)\Sigma_{\mathrm{f}}\phi_{\mathrm{n}}\left(E'\right)dE', \text{ and} \tag{6}$$

$$S_\gamma\left(E\right)=\chi_{\gamma,\mathrm{f}}\left(E\right)\int_0^\infty \bar{y}_{\gamma,\mathrm{f}}\left(E'\right)\Sigma_{\mathrm{f}}\phi_{\mathrm{n}}\left(E'\right)dE'+\chi_{\gamma,\mathrm{nf}}\left(E\right)\int_0^\infty \bar{y}_{\gamma,\mathrm{nf}}\left(E'\right)\left(\Sigma_{\mathrm{t}}-\Sigma_{\mathrm{f}}\right)\phi_{\mathrm{n}}\left(E'\right)dE', \tag{7}$$

where $\chi_{\mathrm{n,f}}$, $\chi_{\gamma,\mathrm{f}}$, and $\chi_{\gamma,\mathrm{nf}}$ are the emission spectrum for fission neutrons, fission photons, and non-fission capture photons, respectively; and $\bar{y}_{\gamma,\mathrm{f}}$, $\bar{y}_{\gamma,\mathrm{nf}}$, and $\bar{\nu}$ are the average yield fission photons, capture photons, and fission neutrons, respectively. Note that we have interpreted the quasi-static factor ($1/k_{\mathrm{eff}}$) to apply only to the number of neutrons emitted per fission ($\bar{\nu}$) and not to the fission reaction rate or the number of photons emitted per fission.

In order to calculate the total heating rate in the reactor, H, an auxiliary equation is needed to relate the local neutron and photon flux (from Eqs.(4)-(7)) to local energy deposition. For convenience, we will write the energy deposition as the sum of three terms,

$$H=H_{\mathrm{f}}+H_{\mathrm{nf}}+H_\gamma, \tag{8}$$

where H_{f} is the direct heating due to fission, H_{nf} is the indirect heating due to neutrons slowing down in the problem (including capture), and H_γ is heating due to photons. These values can be calculated from the average KERMA values described in Section 2.2 along with the neutron and photon fluxes obtained by solving Eqs. (4)-(7). In this paper, we will consider four separate formulations for the energy deposition equation, each of which are described in detail below.

Before proceeding, it should be noted that the use of MC methods for solving fixed-source and eigenvalue radiation transport problems of the form shown in Eqs. (4)-(7) is well-established. In fact, many modern MC transport codes, including MCNP [1], support coupled transport calculations. The objective of this work is to develop a common framework for implementing, and easily switching between, approximate (and exact) energy deposition treatments.

3.1. Treatment 1: Constant Energy Release per Fission

The first energy deposition treatment is to simply assume that a constant amount of energy is released per fission and that all energy is deposited locally at the fission site. This approximation is equivalent to

$$H_{\mathrm{f}}=\int_0^\infty C_1\Sigma_{\mathrm{f}}\phi_{\mathrm{n}}\left(E\right)dE; \qquad H_{\mathrm{nf}}=0; \qquad H_\gamma=0, \tag{9}$$

where C_1 is a user-defined constant, which gives the total sensible energy release per fission (including all indirect energy released during neutron slowing-down). For thermal fission in ^{235}U, values for C_1 typically range between 198 and 207 MeV per fission [2].

In this case, the local energy deposition (power) is directly proportional to the fission density. This relationship is especially convenient because it is independent of the photon flux, thereby eliminating the need for a separate photon transport calculation. However, the approximation does not account for energy redistribution within, or leakage from, the problem, nor does the approximation account for differences in energy released due to spectral shifts or fission of different nuclides. Nevertheless, this energy deposition treatment is widely used for many radiation heating applications due to its simplicity and ease of implementation.

3.2. Treatment 2: Constant Indirect Energy Release per Fission

The second energy deposition treatment also assumes that all energy is created and deposited locally at the fission site. However, this approximation makes use of energy-dependent, nuclide-specific fission energy release (ENDF MT 458 [4]) data provided in nuclear data evaluations to obtain a better estimate of the energy released during each fission event. As a result, the energy release and deposition rates for each category (fission, neutron non-fission, and photon) can be estimated by

$$\begin{aligned} H_{\mathrm{f}} &= \int_0^\infty \left[\sum_i \left(f_{\mathrm{fpke},i} + f_{\mathrm{beta},i} \right) \bar{Q}_{\mathrm{f},i}\left(E\right) \Sigma_{\mathrm{f},i} \right] \phi_{\mathrm{n}}\left(\vec{r},E\right) dE = \int_0^\infty \bar{h}_{\mathrm{f}} \phi_{\mathrm{n}}\left(E\right) dE \\ H_{\mathrm{nf}} &= \int_0^\infty \left[\sum_i \left(\left(f_{\text{prompt n},i} + f_{\text{delayed n},i} \right) \bar{Q}_{\mathrm{f},i}\left(E\right) + C_2 \right) \Sigma_{\mathrm{f},i} \right] \phi_{\mathrm{n}}\left(E\right) dE \\ H_{\gamma} &= \int_0^\infty \left[\sum_i \left(f_{\text{prompt }\gamma,i} + f_{\text{delayed }\gamma,i} \right) \bar{Q}_{\mathrm{f},i}\left(E\right) \Sigma_{\mathrm{f},i} \right] \phi_{\mathrm{n}}\left(E\right) dE \end{aligned} \tag{10}$$

where C_2 is a user-defined constant, which gives the total indirect energy released during neutron slowing down, and i is an index over all nuclides. For thermal fission in ^{235}U, values for C_2 typically range between 3 and 12 MeV per fission [2].

By explicitly accounting for differences in energy released due to changes in the energy spectrum or fission by different nuclides through life, this approximation provides a modest improvement over the previous relationship. Because the relationship remains independent of photon flux, it retains the advantages of the previous approximation. For MC transport methods this approximation is easy to implement if MT 458 nuclear data for each nuclide is available.

3.3. Treatment 3: Local Photon Energy Deposition

The third energy deposition treatment builds upon the previous treatment by adding explicit neutron energy transport, while retaining local photon energy deposition. In this case, fission neutrons carry energy away from the fission site and deposit it along their history. Energy of charged particles produced during fission is deposited locally at the fission site, while neutron slowing-down energy transfer (recoil and charged particle production) is deposited at the site of

each neutron collision. Energy released as photons, due to fission or non-fission neutron capture, is deposited locally at the fission or collision site, respectively. This treatment is equivalent to

$$H_{\mathrm{f}}(\vec{r}) = \int_0^\infty \bar{h}_{\mathrm{f}}\phi_{\mathrm{n}}(E)\,dE; \qquad H_{\mathrm{nf}}(\vec{r}) = \int_0^\infty \bar{h}_{\mathrm{nf}}\phi_{\mathrm{n}}(E)\,dE$$
$$H_{\gamma}(\vec{r}) = \int_0^\infty C_3\left[\sum_i \left(f_{\text{prompt }\gamma,i} + f_{\text{delayed }\gamma,i}\right)\bar{Q}_{\mathrm{f},i}(E)\Sigma_{\mathrm{f},i} + E\chi_{\gamma,\mathrm{nf},i}(E)\bar{y}_{\gamma,\mathrm{nf},i}(E)\left(\Sigma_{\mathrm{t},i} - \Sigma_{\mathrm{f},i}\right)\right]\phi_{\mathrm{n}}(E)\,dE, \tag{11}$$

where C_3 is the user-defined fraction of photon energy that is deposited locally (the remaining photon energy is assumed to leak out of the problem), and

$$\left[\sum_i E\chi_{\gamma,\mathrm{nf},i}(E)\bar{y}_{\gamma,\mathrm{nf},i}(E)\left(\Sigma_{\mathrm{t},i} - \Sigma_{\mathrm{f},i}\right)\right]\phi_{\mathrm{n}}(E), \tag{12}$$

is the average total photon energy produced during a non-fission neutron interaction. Equation (12) can be calculated by NJOY for each target nuclide, by taking the difference between the local and non-local KERMA values [3], as described in Reference 5.

Including energy transport by neutrons provides a significant improvement over the previous approximations. The relationship still neglects photon energy redistribution, (although photon energy leakage can be approximated by the user-defined constant C_3) which eliminates the need for explicit photon transport. However, implementing the approximation so that the kinetic energy carried away by neutrons is preserved between fission generations is challenging, especially for non-critical systems. The challenge is due to the fact that the neutron transport equation is derived from (neutron) mass balance rather than energy balance. Applying the quasistatic correction factor ($1/k_{\mathrm{eff}}$) to the fission neutron production term forces the neutron population to be at steady state, but creates a mismatch between the neutron energy released in fission and the actual energy carried away by neutrons. As a result, the total kinetic energy of neutrons is biased in proportion to $1/k_{\mathrm{eff}}$; high for subcritical systems, and low for supercritical systems. In order to preserve energy between generations, an energy rebalance step is required, which is separate from the standard population normalization. The energy rebalance will be discussed further in the next section.

3.4. Treatment 4: Coupled Radiation Transport (Full Transport)

Fully coupled neutron-photon radiation transport provides the highest level of fidelity for modeling energy deposition. This increased fidelity comes with a computational cost, since this treatment requires explicit energy transport for both secondary neutrons and photons. The details for this treatment are identical to the previous approximation, except that energy released as photons (both fission and capture) is not assumed to be deposited locally. The full transport energy deposition treatment can be written as

$$H_{\mathrm{f}} = \int_0^\infty \bar{h}_{\mathrm{f}}\phi_{\mathrm{n}}(E)\,dE; \qquad H_{\mathrm{nf}} = \int_0^\infty \bar{h}_{\mathrm{nf}}\phi_{\mathrm{n}}(E)\,dE; \qquad H_{\gamma} = \int_0^\infty \bar{h}_{\gamma}\phi_{\gamma}(E)\,dE, \tag{13}$$

where the $\bar{h}$ values are the average KERMA values described in Section 2.2. Unlike the previous heating approximations, the photon heating component of Eq. (13) requires the photon

flux, ϕ_γ. In order to calculate the photon flux, a neutron transport calculation must be run first, in order to obtain an estimate of the neutron flux ϕ_n, which can then be used in Eq. (7) to generate a source for the subsequent fixed-source photon transport calculation. The need for two separate transport calculations increases the computational cost of the full transport heating treatment relative to the previous three approximations. However, the expense of a full-fidelity heating calculation can be partially mitigated through the use of a photon redistribution function, ω. The photon redistribution function, which is defined by

$$\omega = \frac{\int_0^\infty \bar{h}_\gamma \phi_\gamma(E)\,dE}{\int_V \int_0^\infty E S_\gamma(E)\,dE\,d\vec{r}}, \tag{14}$$

gives the local energy deposition (as a function of spatial position) normalized by the total energy of source photons emitted. Multiplying the photon redistribution function by the total energy of photons released during neutron transport gives the photon energy deposition as a function of the neutron flux only,

$$H_\gamma = \omega \int_V \int_0^\infty \left[\sum_i \left(f_{\text{prompt }\gamma,i} + f_{\text{delayed }\gamma,i} \right) \bar{Q}_{\text{f},i}(E) \Sigma_{\text{f},i} + E \chi_{\gamma,\text{nf},i}(E) \bar{y}_{\text{nf},i}(E) \left(\Sigma_{\text{t},i} - \Sigma_{\text{f},i} \right) \right] \phi_n(E)\,dE\,d\vec{r}. \tag{15}$$

By normalizing to the total photon source energy rather than the source intensity, the photon distribution function simplifies the process of correctly normalizing the photon source term to ensure consistency, and therefore preserve energy balance, with respect to the neutron transport calculation. Furthermore, once calculated and saved, the photon redistribution can be used in Eq. (15) to estimate the photon energy deposition term without the need for additional photon transport calculations. Thus, for problems where the shape and spectrum of the photon source distribution are changing slowly, explicit photon transport is not necessary for every neutron transport calculation. The ability to reuse the same photon redistribution function for many separate neutron transport calculations offers a way to improve the efficiency of the full transport energy deposition treatment for multi-timestep and/or iterative non-linear feedback calculations.

4. IMPLEMENTATION IN MONTE CARLO PARTICLE TRANSPORT METHOD

The derivations of the energy deposition framework and deposition approximations presented in Section 3 are very general and the framework could, in principle, be used for both deterministic and stochastic transport methods. In this section, we present implementation details for using the framework with a continuous-energy MC neutron/photon transport method. For testing purposes the framework and all four energy deposition treatments were implemented in the in-house MC code MC21 [6] and the details of the implementation are presented below.

Many of the individual heating rates for the four energy deposition treatments, Eqs. (8)-(13), are simply moments of the neutron or photon flux. These quantities can be scored during MC transport using traditional collision or track length estimators.

For calculations that use either of the energy deposition treatments that allow energy transport via neutrons (Full Transport and Local Photon Energy Deposition), an energy rebalance factor

must be calculated for each generation of neutrons. During eigenvalue calculations, the fission neutron source must be renormalized between generations, in order to prevent the bank size from becoming too large or too small. In MC21, the fission source renormalization is achieved by adding or removing extra source sites to the fission bank until the desired bank size is reached. However, for non-critical systems, this source renormalization causes an imbalance between the total energy of neutrons released during fission and the total energy of neutrons in the normalized source bank for the subsequent generation. This imbalance is due to the fact that the source normalization only preserves the total number of neutrons followed during any generation, and is not intended to enforce energy balance. In order to correct for this fact, we compute an energy rebalance factor for each neutron generation by taking the ratio of the total neutron energy released in fission during the previous generation to the total neutron energy in the normalized source bank for the current generation. This energy rebalance factor serves as a weighting factor for energy deposition and leakage tallies, which preserves total fission neutron energy across generations. It is important to recognize that the energy rebalance factor does not affect the energy of any individual neutron. Instead, the factor acts as a statistical weight, allowing each particle in the source bank to represent more (for supercritical problems) or fewer (for subcritical problems) neutrons for energy balance purposes only. In practice, the energy rebalance factor should always be close to the estimated eigenvalue for the corresponding generation.

The full transport energy deposition treatment requires both neutron and photon transport calculations. Unlike some MC solvers, such as MCNP, which run the secondary photons immediately following their parent particle during a single transport simulation, MC21 separates the neutron and photon transport into two separate calculations. When a full transport energy deposition calculation is executed, MC21 first runs a neutron transport calculation. During the transport calculation the code samples capture and fission photons at every neutron collision event and writes information about these photon source sites to an HDF5 census data file. Following the neutron transport calculation, MC21 then runs a photon transport calculation using the source data from the photon source data census file. During photon transport, MC21 computes the energy deposition for each cell in the problem using the local photon KERMA value $\bar{h}_\gamma$. Following the calculation, the code normalizes these energy deposition values by the total photon source energy released to compute the relative photon energy deposition fraction for every cell in the problem. This cell-based energy deposition fraction data forms a discretized representation of the photon redistribution function, which describes how photons will redistribute energy throughout the problem via transport. Once calculated, the photon redistribution function is multiplied by the total photon energy released during the neutron calculation and the resulting product is summed over all cells to give an estimate of the total photon energy deposition, per Eq. (15). This photon redistribution function is also saved so that the local photon energy deposition can be quickly recalculated based only on the total photon energy released in a subsequent neutron calculation. Thus, photon transport calculations only need to be run when changes in the problem (due to depletion, thermal feedback, etc.) have caused a change in the overall shape of the photon redistribution function.

During transport, MC21 keeps track of the total (sensible) energy released during each particle history, as well as the fraction of this energy that is actually deposited within the problem. This global energy release and deposition information gives a measure of the total energy production of a system, per starting neutron. The estimated global energy deposition per starting neutron

result provides an important link between the normalized MC21 tally results (reported per starting neutron) and a more meaningful absolute result, which has been scaled to a given power level. In eigenvalue calculations, MC21 automatically calculates a flux normalization factor by dividing the user-defined power for the problem by the estimated global energy deposition per starting neutron,

$$T = \frac{P}{\int_V H \, d\vec{r}}, \tag{16}$$

where P is the user-input power level and H is the per-starting-neutron-normalized energy deposition function defined in Eq. (8). The resulting flux normalization factor, T, is reported with units of [starting neutrons/second], and serves as a scaling factor for converting raw MC results into absolute results at the specified power level for the system.

5. RESULTS

The in-line energy deposition framework, along with all four energy deposition formulations, was implemented in a developmental version of MC21, a continuous-energy MC particle transport code [6]. The accuracy and performance of the various energy deposition treatments were assessed through testing on a simplified 1-D model of a homogenized reactor core surrounded by a simple compound shield containing polyethylene and lead. The test model consists of a 10 cm half-thickness core region containing a homogenized mixture of 3% enriched UO_2 and light water, with an H/U ratio of 11.64. The homogenized core is surrounded by 60 cm of polyethylene (CH_2), 20 cm of lead (^{204}Pb, ^{206}Pb, ^{207}Pb, and ^{208}Pb, with natural abundances), and 10 cm of vacuum. The bound-nuclide (moderator) cross-section evaluations for H-H_2O and H-Poly were for hydrogen in the core and polyethylene regions, respectively. The model is 20 cm thick in the y and z dimensions, with reflective boundary conditions applied to the maximum and minimum y and z-planes, creating a 1-D problem. In the x-dimension, a reflective boundary condition is applied at the core centerline ($x = 0$) and an escape boundary condition is applied at the outer edge of the vacuum region ($x = 100$). The eigenvalue for the model was computed to be $k_{\text{eff}} = 1.0390 \pm 0.0002$ (95% confidence interval).

MC21 was used to run energy deposition calculations with this model using the four energy deposition treatments described in Section 3. Each calculation used 5,100 batches (first 100 discarded) of 10,000 neutron histories, for a total of 50 million active histories. The coupled neutron-photon transport calculation used 50 million histories for both the neutron and photon calculations. During the simulation, tallies for flux, radiation absorption, energy release (by category), and energy deposition (by category) were collected over a uniform 1000 bin mesh ($\Delta x = 0.1$ cm). Energy deposition results for all calculations were normalized to a total thermal power level of 1 Watt. The user-input parameters used for the approximate energy deposition treatments were: 201 MeV/fission constant energy released per fission (Treatment 1), 7.5 MeV/fission constant indirect energy release per fission (Treatment 2), and 100% local photon energy deposition (Treatment 3). All calculations were run in parallel on 16 quad-core Intel Xenon Nehalem E5530 processors running at 2.4 GHz (64 cores total).

Table I. Run time and calculated energy deposition fraction by region for each of the energy deposition treatments.

	Constant Energy per Fission	Constant Indirect Energy per Fiss.	Local Photon Energy Dep.	Fully Coupled Transport
Total Run Time	**582.08 s**	**580.76 s**	**587.89 s**	**1414.65 s**
Neutron Calc.	582.08 s	580.76 s	587.89 s	958.08 s
Photon Calc.	-	-	-	456.57 s
Energy Deposition Fraction by Region				
Core Total	**100%**	**100%**	**98.85%**	**97.37%**
Neutron	100%	93.55%	90.25%	90.24%
Photon	-	6.45%	8.60%	7.12%
Polyethylene Total	**-**	**-**	**1.15%**	**2.49%**
Neutron	-	-	0.526%	0.527%
Photon	-	-	0.626%	1.96%
Lead Total	**-**	**-**	**2.87×10^{-5}%**	**0.14%**
Neutron	-	-	2.39×10^{-6}%	2.31×10^{-6}%
Photon	-	-	2.63×10^{-5}%	0.135%

Table I gives the simulation run-time and energy deposition fraction, by region and radiation type, for each of the four energy deposition treatments. The results show that the three approximate energy deposition treatments (Treatments 1-3) run at the same speed, while the coupled transport calculation runs ~2.5 slower. This slowdown is due to two reasons: the coupled calculation requires an explicit photon transport calculation, and the neutron transport calculation takes longer because the code must sample and store photon source sites at every neutron collision.

The results in Table I also show the effects of the various approximations on energy deposition. The first two approximations deposit all energy within the core region due to the underlying assumption that all energy is deposited at the fission site. Even with this crude approximation, the estimated energy deposition in the core region is within 3% of the reference value (coupled neutron-photon transport). However, without energy transport, the first two energy deposition approximations cannot estimate the heating in the ex-core shielding material. The third approximation, local photon energy deposition, includes energy transport due to neutrons, and is able to calculate heating in the polyethylene and lead shields with a negligible increase in run time. Because this approximation neglects the photon transport, which is the dominant heating mechanism in the lead and deep in the polyethylene, the heating estimates substantially under predict the energy deposition rates in these regions. Based on the integral results shown in Table I, it appears that all four energy deposition treatments will produce reasonable (but high) heating estimates within the core region. However, the three approximate energy deposition treatments fail to accurately predict ex-core heating rates. This shortcoming is emphasized in the compound shield test problem used in these tests, which emphasizes photon transport away from the core. In models where neutron moderation and stopping occurs in high-Z materials (or a

heterogeneous mixture of high and low-*Z* materials, such as in a lattice of fuel pins) the local photon energy deposition approximation is expected to show better agreement with a coupled transport reference solution.

In addition to considering integral heating results by region, Figures 1 and 2 illustrate the energy deposition density, in Linear and Log scale, respectively, as a function of spatial position for each of the four energy deposition treatments. Inspection of these figures shows that all four methods show excellent agreement in the core region, with energy deposition closely following the fission distribution. Local energy deposition rates for the three approximate energy deposition treatments range from 1% to 6% higher than the reference solution obtained from the coupled transport calculation.

6. CONCLUSIONS

A generalized framework for the in-line treatment of energy deposition in MC transport calculations has been developed and tested. This framework gives users the flexibility to select, at run-time, from among four energy-deposition treatments with varying levels of fidelity. Each energy-deposition treatment uses a unique set of self-consistent approximations, which ensure that energy balance is satisfied over the entire problem. The constant energy release per fission and constant indirect energy release per fission treatments assume local energy deposition at the fission site and rely on user-input values for the energy release. The local energy deposition treatment includes neutron energy transport but assumes photon energy is deposited where created. Finally, the fully-coupled neutron-photon transport treatment includes explicit energy transport by both neutrons and photons. This flexibility to tailor the accuracy of the energy deposition treatment to a particular application or to meet resource limitations has the potential to increase computational throughput and/or enable energy deposition calculations for larger models than ever before.

All four of the energy deposition treatments were tested on a simple 1-D homogenized core/compound shield benchmark problem. All of the energy deposition treatments were able to predict the integrated energy deposition in the core to within 3% and the local heating density in the core to within 6%, relative to a reference solution. The three approximate energy deposition treatments (constant energy per fission, constant indirect energy per fission, and local photon deposition) ran at similar speeds, and were 2.5 times faster than the reference coupled neutron-photon transport method. However, all three of the approximate methods significantly underpredicted the energy deposition deep in the compound shield. These results indicate that approximate energy deposition treatments may be suitable for some types of in-core analysis, but are not practical for systems with significant energy redistribution due to photon transport.

ACKNOWLEDGEMENTS

The authors would like to thank the MC21 development team at the Bettis and Knolls Atomic Power Laboratories for their valuable assistance with this work. In particular, Hansem Joo (Bettis) and Ed Caro (KAPL) provided valuable advice and testing during the development of the generalized energy deposition method. In addition, Tim Trumbull (KAPL) and Reza Gouw (Bettis) provided nuclear data support for this effort.

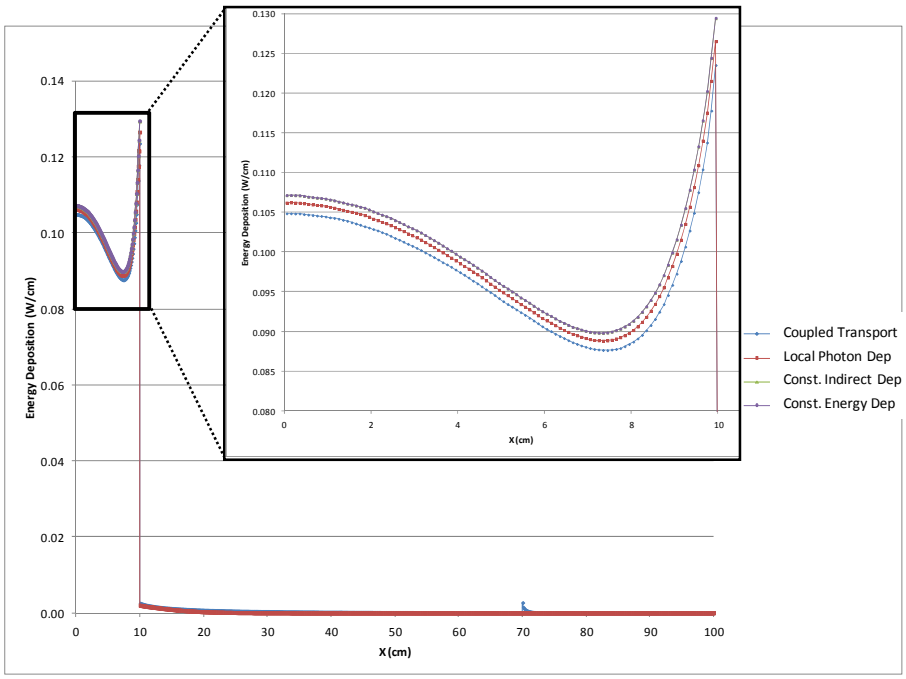

Figure 1. Energy deposition density as a function of position for each of the four energy deposition treatments (linear scale). The results for the constant energy per fission treatment and the constant indirect energy per fission treatment are indistinguishable.

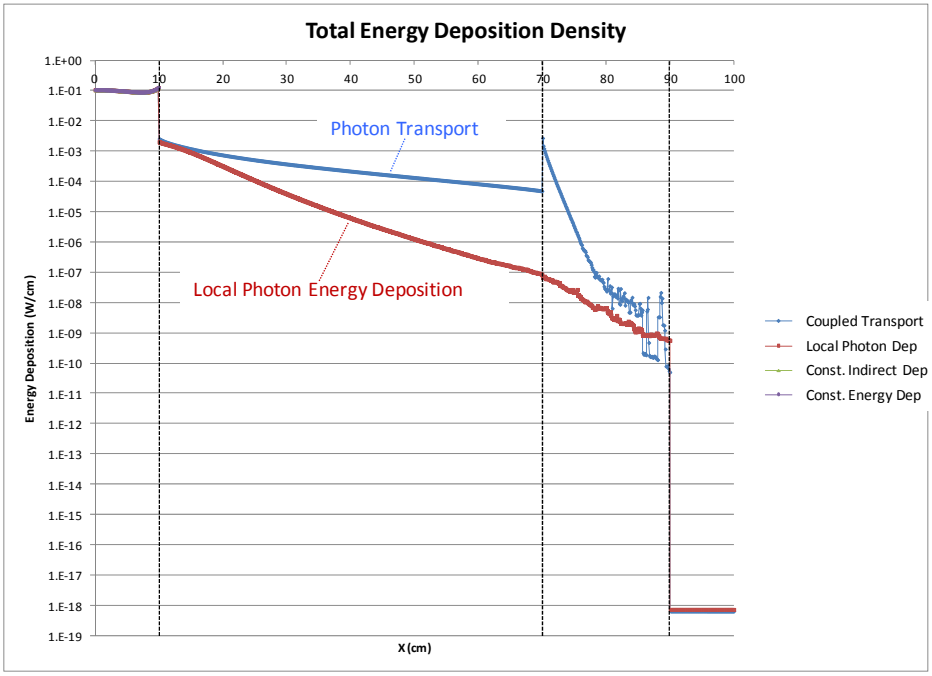

Figure 2. Energy deposition density as a function of position for each of the four energy deposition treatments (log scale). The results for the constant energy per fission treatment and the constant indirect energy per fission treatment are indistinguishable.

REFERENCES

1. X-5 Monte Carlo Team, "MCNP – A General Monte Carlo N-Particle Transport Code Version 5," *Technical Report LA-UR-03-1987*, Los Alamos National Laboratory Report (2003).
2. J.R. Lamarsh, Introduction to Nuclear Engineering, 2nd Ed., Addison-Wesley, Reading, MA (1983).
3. R. E. MacFarlane and D. W. Muir, "The NJOY Nuclear Data Processing System, Version 91," Los Alamos National Laboratory, LA-12740-M (1994).
4. M. Herman, A. Trkov, "ENDF-6 Formats Manual, Data Formats and Procedures for the Evaluated Nuclear Data File ENDF/B-VI and ENDF/B-VII," ENDF-102, BNL-90365-2009, National Nuclear Data Center, Brookhaven National Laboratory, Upton, NY (2009).
5. T.H. Trumbull, "Nuclear Data Processing for Energy Release and Deposition Calculations in the MC21 Monte Carlo Code," *Int. Conf. on Mathematics and Computational Methods Applied to Nuc. Sci. and Eng.*, Sun Valley, Idaho, May 5–9 (2013).
6. T. M. Sutton, *et al.*, "The MC21 Monte Carlo Transport Code", *Proc. Joint Int. Topical Meeting on Mathematics & Computation and Supercomputing in Nuclear Applications*, Monterey, California, April 15–19 (2007).